Chemical Engineering Science 285 (2024) 119590

Contents lists available at ScienceDirect

Chemical Engineering Science

journal homepage: www.elsevier.com/locate/ces

3D printed zeolite monoliths as open-source spare parts for oxygen concentrators

Florinda Coro [a], Licia Di Pietro [b], Simone Micalizzi [a], Antonio Bertei [c], Giuseppe Gallone [c], Anna Maria Raspolli Galletti [d], Arti Ahluwalia [a,e], Carmelo De Maria [a,e,*]

[a] Research Center E. Piaggio and Dpt. of Information Engineering, University of Pisa, Pisa, Italy
[b] 1MED S, Agno, Switzerland
[c] Dpt. of Civil and Industrial Engineering, University of Pisa, Pisa, Italy
[d] Dpt. of Chemistry and Industrial Chemistry, University of Pisa, Pisa, Italy
[e] Ubora Association, Italy

ARTICLE INFO

Keywords:
Oxygen concentrator
3D printed zeolite
Open-source spare parts
Adsorption process
Zeolite monoliths

ABSTRACT

Oxygen concentrators are essential medical devices for basic emergency care, surgery and treatment for chronic and acute respiratory diseases. Despite their reliability and accessibility, they require spare parts which can be difficult to source in low resource settings, where the extreme environmental conditions and the overloads often make failures more frequent. The solution to this shortcoming can be their local production, enabled by 3D printing (3DP) technologies. Here we describe an extrusion-based 3DP process to produce zeolite monolith structures for use in the air adsorption process. The printed structures were physically and mechanically characterized. Compared to the material in pelletized form, the 3D printed zeolite monoliths have better transport properties (30 times increased permeability), comparable adsorption (being comparable with standard pellets), and are easier to handle. They are therefore the more appropriate technology for higher performance, easier maintenance, and lower weight oxygen concentrators in low resource settings.

1. Introduction

Oxygen is an essential element of basic emergency care, and it is required for surgery and treatment of several chronic and acute respiratory diseases (Wandi et al., 2006). However, it is often scarce in low-resource settings (LRS) (Enarson et al., 2008). Field studies show that reasons for the scarcity of oxygen are frequently associated with cost and lack of infrastructure to install and maintain a reliable oxygen supply (Hill et al., 2009). But even where oxygen supplies are available, patient access may be limited due to missing accessories, inadequate electricity and/or shortage of trained staff (Di Pietro et al., 2020).

An oxygen concentrator can produce up to 82 % concentrated oxygen through the Pressure Swing Adsorption (PSA) process (World Health Organization., 2020). The PSA cycle operates at ambient temperature with super atmospheric pressure (up to 4 atm (Sami et al., 2022). At these pressures, nitrogen gas N_2 is removed from the air by adsorption, typically on zeolite sieve beds (Sami et al., 2022). Consequently, the gas is enriched in O_2 to be delivered to the patient. After use, the bed is regenerated by lowering the pressure to 1 atm causing the release of the adsorbed N_2 (World Health Organization., 2016).

Efficient operation of the PSA process is necessary to maximize the capacity of the adsorbent bed and reduce the power requirements (Sircar, 2002). In fact, oxygen concentrators require regular maintenance and a reliable power supply (World Health Organization., 2016). Typically, a pair of sieve beds must be changed every 18–24 months, but in cases of intense use (12–18 h per day), beds must be replaced after 12–16 months (Bradley et al., 2015).

The current systems for N_2 removal in oxygen concentrators utilize fixed sieve beds, organized in two columns, a compressor, and several valves to control the pressure cycling and flow sequence of atmospheric air entering the system (Ackley, 2019). The columns and the compressor are the two main factors contributing to the size and weight of an oxygenator (Ackley, 2019). A decrease in adsorbent particle size markedly increases the pressure drop along a column packed with small-size adsorbent particles (Ackley, 2019). This in turn requires higher blower power to maintain gas flow which leads to more frequent calls for system maintenance (Ackley, 2019). To reduce flow resistance through the fixed bed, pelletization of adsorbent particles with clay

* Corresponding author at: Research Center E. Piaggio and Dpt. of Information Engineering, University of Pisa, Pisa, Italy.
E-mail address: carmelo.demaria@unipi.it (C. De Maria).

https://doi.org/10.1016/j.ces.2023.119590
Received 9 August 2023; Received in revised form 13 November 2023; Accepted 30 November 2023
Available online 3 December 2023

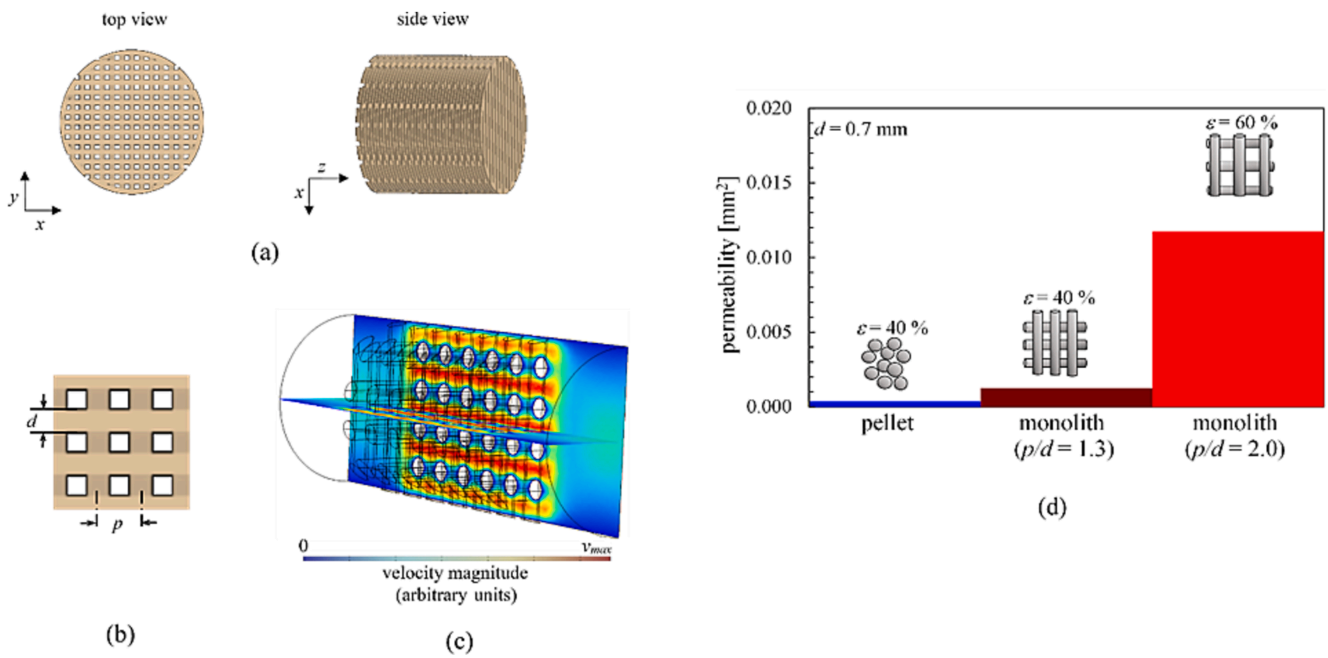

Fig. 1. Permeability of monolith structures assessed via fluid flow simulations: (a) top and side views of the monolith structures; (b) detail view of the monolith geometry; (c) simulated velocity distribution in laminar regime; (d) permeability of pellet and monoliths for different p/d ratios and porosities ε for a given diameter.

binder (or binderless pellets) is required (Zapata Ballesteros et al., 2022). The pellets are highly porous structures, allowing a more rapid mass transfer through the pellet (Zapata Ballesteros et al., 2022). However, this open composite structure can be weakened by humidity and/or large temperature excursions. Moreover, dusting due to particle attrition in closed environments can lead to human health problems, such as pneumoconiosis (Safety and Administration, 2010). To improve N_2 removal system efficiency and reliability, more robust and more efficient adsorbents are required, such as monolithic structures (Thakkar et al., 2016; Mosca et al., 2010; Rezaei et al., 2010; Rezaei and Webley, 2010). Monoliths are structured materials with parallel gas flow channels in which the shape and the diameter of the parallel channels, as well as their density per cross-sectional area of the monolith, can be controlled through conventional extrusion processes (Li et al., 1998). In this regard, Li et al., in their study, reported that comparing monoliths performance with pellets performance in an oxygen adsorption process, monoliths, fabricated by an extrusion process, present enhanced performance in terms of pressure drop, pressurization time, attrition resistance macropore structure and axial dispersion coefficient. In addition, using monoliths instead of pellets, there is not an increase in temperature during the pressurization cycle (Li et al., 1998). Several other studies reported the use of monoliths for gas separation but not related to oxygen enrichment (Thakkar et al., 2018; Thakkar et al., 2016; Liu et al., 2021).

Most medical equipment is manufactured in high-income countries and is designed to operate in clean, sterile, climate-controlled environments, with reliable electricity (Di Pietro et al., 2020). However, in LRS, medical devices (MDs) are subjected to harsh environmental conditions including extreme climates, humidity, dust, and power supply instability (Piaggio et al., 2019). These conditions cause more frequent failures and consequently higher requests for spare parts, which are expensive and difficult to find. Indeed, devices often stop working as soon as the first replacement part is required (Richards-Kortum and Oden, 2013). As a result, maintenance and repair are as problematic as acquisition (Malkin, 2007). Studies conducted by Engineering World Health revealed that hospitals in LRS find it easier to request a new oxygen concentrator from their sponsors than to spend \$5 to repair a concentrator already in their possession (Malkin, 2007).

Additive manufacturing technologies, commonly known as 3D printing (3DP), are increasingly relevant in the biomedical field, particularly in the production of bespoke medical products and equipment, such as customized surgical tools (Banks, 2013), prostheses (Frame and Huntley, 2012), implants (Mahaisavariya et al., 2006; Sheth et al., 2015), and anatomical models for surgical planning (Rengier et al., 2010). Apart from customization, benefits provided by the application of 3DP in healthcare include increased cost efficiency (Schubert et al., 2014), productivity, and collaboration (Ahluwalia et al., 2018; Ahluwalia et al., 2018). In a context where MD suppliers and manufacturers do not always have a satisfactory solution in maintenance cases involving spare parts (e.g., no more after-sales service on old MDs still in operation, sales of complete kits instead of single spare parts, overpricing of spare parts), and considering the constraints of maintenance workshops in hospitals (e.g., limited storage capacity and long delivery times), 3DP for MD spare parts can be a viable solution for biomedical maintenance teams.

Most recently, 3DP technologies have been in demand for fabricating complex geometries with unique mechanical and structural properties (Zhou and Bhaduri, 2019). Notably, unlike conventional extrusion processes, these technologies allow for precisely fabricating 3D structures with desired configurations and optimized properties (Rezaei and Webley, 2010). Higher flexibility at lower implementation costs is another notable advantage of these methods (Zhou and Bhaduri, 2019). Using 3DP, monoliths with various cross sections, wall thicknesses, and channel sizes, including lateral pores can be fabricated to achieve a fully connected lattice structure.

Given this scenario, this study aims to provide a structured process for the in loco design and production of spare parts for an oxygen concentrator. To the best of our knowledge, there are no other studies published in the literature in which 3DP techniques are used to obtain spare parts for oxygen concentrators enabling local manufacturing and presenting enhanced characteristics in terms of adsorption properties. Particular attention has been paid to computer-aided modelling and fabrication of concentrator absorbent sieve beds based on zeolite monolith structures. An extrusion-based 3DP process was identified as the enabling technology to produce the monoliths as single solid structures with many interconnected macroporous channels. The design and

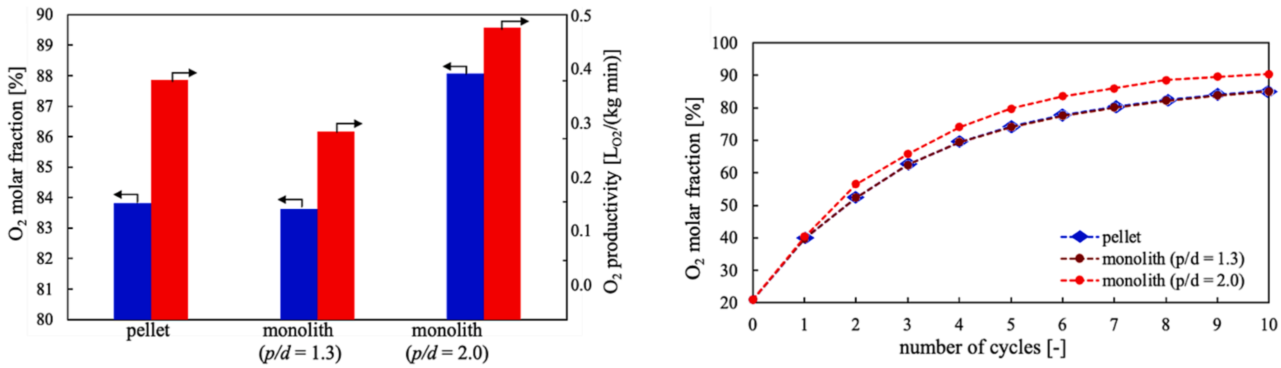

(a)   (b)

Fig. 2. Simulation of a two-bed oxygen concentrator with pellet or monolith adsorbents with the same diameter d = 0.7 mm: (a) average oxygen molar fraction and productivity at periodic steady-state; (b) oxygen purity as a function of the number of cycles during the start up of the oxygen concentrator.

manufacture pipeline was supported by the UBORA platform, where the project is documented (Di Pietro et al., 2019; UBORA, 2023). UBORA guides the identification of clinical needs, product requirements and relevant standards (in Supplementary information), promoting a collaborative and open-source design (Spare Parts for Oxygen Concentrators, 2023).

Here we describe the pipeline starting from the mathematical modelling, design, fabrication, and characterization of the zeolite monoliths. Process validation, a crucial element of the pipeline, was accomplished by evaluating the performance of a commercial oxygen concentrator loaded with zeolite monolith structures.

2. Mathematical modelling

The rational manufacturing of monolithic adsorbents can benefit from the guidance of modelling techniques. Physics-based modelling provides design indications for maximising the permeability and performance of monolithic structures as a function of their micro-architecture. Optimal design allows reducing pressure losses and once a geometry has been established, the oxygen concentration capabilities of monoliths can be predicted. Both these objectives are explored in this section.

The permeability of the monoliths was evaluated by simulating fluid flow in a three-dimensional representation of the monolith microstructure, as reported in Fig. 1.The monolith structure under consideration is represented as a net of cylindrical fibers arranged in a regular square pitch, as shown in Fig. 1(a). A representative portion of the geometry was drawn in 3D in the finite-element software COMSOL Multiphysics v. 6.1 (Inc, 2019) for different values of fiber diameter d and pitch p (Fig. 1 (b)). The Navier-Stokes equations were solved in laminar regime by using the creeping flow interface in COMSOL Multiphysics; the fluid velocity and flow rate were obtained upon application of an arbitrary small pressure difference at the ends of the computational domain (Fig. 1(c)). The monolith permeability was then evaluated using Darcy's law (Zaman and Jalali, 2010). A systematic analysis of monolith permeability and other effective transport properties as a function of the pitch-diameter ratio (p/d) is reported in the Supplementary Materials (Fig. S1). Fig. 1(d) compares the permeability of a conventional pellet made of randomly dispersed spherical particles (Wang et al., 2020) with the permeability of two monoliths with different pitch-diameter ratios chosen to have either the same porosity ε of the pellet (ε = 40 % for p/d = 1.3) or a larger porosity (ε = 60 % for p/d = 2.0). Both the spherical pellets and the fibers are assumed to have the same diameter in order to compare them in equivalent conditions; more specifically, the selected diameter is d = 0.7 mm, equal to the fiber diameter of the monolith zeolites fabricated in this study. Our results show that the permeability increases by a factor of 3 for a monolith with the same porosity as the pellet, up to a factor 30 if the p/d of the fibers is set to 2. Hence, the simulations indicate that the monolith structures can significantly reduce pressure drops in an oxygen concentrator.

The potential of using monoliths in an oxygen concentrator was further assessed by simulating the pressure swing adsorption process in a two-bed axial adsorber. The mathematical model of the oxygen concentrator is based on mono-dimensional time-dependent conservation equations for oxygen and nitrogen, both in the gas and adsorbed phases (i.e., the zeolite), coupled to the conservation of momentum in the gas phase and to the adsorption/desorption kinetics of oxygen and nitrogen. Two beds working in parallel are simulated, following a four-step Skarstrom cycle (pressurization, adsorption, blowdown and purge) (Wang et al., 2020). The beds replicate the geometry of the monoliths and oxygen concentrator and are shifted in time by half a cycle each, so that the first bed is purged when the second undergoes the adsorption step, and vice versa. Gas adsorption parameters are taken from Wang et al. (Wang et al., 2020). The model is solved until the periodic steady-state operation is attained, enabling the evaluation of the oxygen molar fraction and productivity. Further details on the model and parameters are reported in the Supplementary Materials.

Pellet and monolith performances were compared by changing the microstructural properties of the bed structures, such as porosity and permeability as described above. Fig. 2(a) summarizes the main performance indicators as obtained from the numerical simulation at the periodic steady-state operation. The figure shows that both pellet and monoliths enable an oxygen purity larger than the minimum requirement of 82 % (left axis, blue bars). Nevertheless, monoliths can achieve comparable or even larger O_2 molar fraction compared to the pellet, even close to 90 % in case of a monolith with p/d = 2. This can be attributed to the larger permeability of the monolith structures (see Fig. 1(d)). The oxygen productivity of the concentrator, expressed per unit mass of zeolite, is also reported in Fig. 2(a) (right axis red bars). In the conditions considered in this comparison, our simulations indicate that the monolith structure with p/d = 1.3 gives a lower oxygen yield compared to the conventional spherical pellet. Note that while the bed porosity ε of the pellets is dictated by the random arrangement of spherical particles, resulting in a porosity constrained in the range of 40 % (Von Seckendorff and Hinrichsen, 2021; Chueh et al., 2014), monoliths can be fabricated in a range of bed porosities by changing the pitch-diameter ratio. In particular, by increasing p/d to 2 results in a bed porosity of 60 % (which is not achievable by any stable random arrangement of spherical pellets (Von Seckendorff and Hinrichsen, 2021), the monolith can provide an increased oxygen productivity per unit of zeolite mass (Fig. 2(a), in red) in addition to a higher oxygen purity (Fig. 2(a), in blue). In addition, the simulations in Fig. 2(b) show

Table 1
Zeolite monoliths: composition and acronyms.

Acronym	Zeolite (wt%)		Printable (Bonatti et al., 2021)	Calcination @ 600°Cfor 3 h
Z50BL	50	Bentonite in LUDOX	Yes	–
Z50BL_C	50	Bentonite in LUDOX	Yes	Yes
Z70BL	70	Bentonite in LUDOX	Yes	–
Z70BL_C	70	Bentonite in LUDOX	Yes	Yes
Z50A	50	Alginate solution	No	–
Z70A	70	Alginate solution	Yes*	–
Z70A_C	70	Alginate solution	Yes*	Yes
Z70BLA	70	Bentonite in LUDOX + Alginate solution	Yes	–
Z80BLA	80	Bentonite in LUDOX + Alginate solution	Yes	–
Z85BLA	85	Bentonite in LUDOX + Alginate solution	No	–

* Collapse of pores in the XZ and YZ plane.

that the oxygen concentrator filled with monolith with p/d = 2 (in light red) reaches its maximum oxygen concentration capacity faster than the monolith with p/d = 1.3 (in dark red) and to the pellet (in blue). In fact, the p/d = 2 monolith allows higher oxygen purity in a lower number of cycles compared to the other adsorbents because of its higher permeability. The oxygen concentration increases faster and the periodic steady-state operation is achieved in a lower number of cycles. Given the faster dynamics of the monolith with p/d = 2, an acceptable oxygen concentration and productivity may be obtained by reducing the feed pressure and by shortening the step times.

In summary, our simulations indicate that given their higher permeability, monoliths have the potential to improve oxygen concentration and oxygen yield with respect to conventional sieve beds. This implies less demanding operating conditions and suggests that monolith-based devices could be designed substantially lighter than current systems and with smaller compressors.

3. Materials and methods

3.1. Materials

Self-standing zeolite monoliths were prepared from 13X zeolite powder (Molecular sieves, 13X, powder, Alfa Aesar®, USA). The powder was mixed with bentonite clay (NanoclayNanomer® PGV, Sigma-Aldrich, Italy) as a binder, a watery binder suspension containing colloidal silica (Ludox HS-40, Sigma-Aldrich, Italy) as a co-binder, and/or Alginate (Alginic acid sodium salt from brown algae, MW 1200–1800 Da, Sigma-Aldrich, Italy) as a plasticizing organic binder. The material characteristics are described in the Supplementary Material (Table S2) for Zeolite 13X, Bentonite, Colloidal silica, and Alginate, respectively.

3.2. Monolith fabrication

3.2.1. Paste preparation

To investigate the adsorption performance of monolithic structures, zeolite 13X monoliths were prepared by varying the zeolite-to-binder weight ratio and the co-binder and plasticizer concentrations as shown in Table 1.

Three binder systems were tested. The first system was composed of an Alginate solution 10 % w/v in distilled water. A second binder system was composed of a paste of bentonite in LUDOX watery binder, prepared by stirring for 10 min at room temperature and amount of bentonite to have a final percentage equal to 50 % w/w of zeolite. A third system was obtained by mixing the two previous binder systems in a 1:1 v/v ratio. For each zeolite-binder compositions, a paste of 13X Zeolite in distilled water (milliQArium ® mini, Sartorius, Germany) was first prepared by sonicating for 10 min with a VC130 sonication probe (Sonics and Materials, Inc, USA). Then the final slurry (i.e., the mixture ready to be 3D printed) was obtained by mixing the zeolite paste with the specific binder system and sonicating again for 30 min.

Air bubbles could cause defects in the later stages of extrusion and in the successive drying and heating steps as described in the next paragraph, and so they were removed by degassing. The paste was stored at 4 °C in a refrigerator for at least 24 h to improve its plasticity, homogeneity, and workability (Ali et al., 2021).

3.2.2. 3D printing process

The monoliths were fabricated using a custom extrusion-based 3D printer. A motor driven plunger was used to extrude the zeolite slurry through a 5 mL syringe fitted with a conical nozzle (final diameter 0.7 mm) (Bon et al., 2021; Chiesa et al., 2020). A cylindrical monolith structure (20 mm × 20 mm × 15 mm) was designed in SolidWorks®, exported as a.stl file, and sliced by Slic3r® - which automatically generates the GCode for the 3D printer. The printing parameters, reported in the Supplementary Materials, allow the fabrication of a 0°-90° layer-by-layer woodpile structure, with a pore diameter of 0.7 mm and a theoretical p/d = 2. As it was considered crucial to obtain reproducible structures with a well-defined shape, fiber size and porosity, prior to fabricating the monoliths, a rapid screening for printability as a self-supporting 3D printed structure was performed (Bonatti et al., 2021). Unprintable compositions were discarded immediately as reported in Table 1.

3.2.3. Thermal curing

After the 3DP process, the monoliths were stored in the fridge at 4 °C for 48 h (Ali et al., 2021). Then they were dried in a controlled atmosphere (20 °C and 80 % relative humidity for 48 h) to partially remove water content. Finally, they were placed in an oven to remove the rest of the water, ramping up the temperature from 30 to 60 °C (heating rate 10 °C/h) for 3 h. This thermal curing protocol was monitored by weighing the samples every hour (at 30, 40, 50, and 60 °C). Bentonite/Ludox and Alginate samples were also subject to calcination at 600 °C for 3 h (heating rate 10 °C/h) to remove the binders and evaluate their effects on the absorption properties of the zeolite.

3.3. Monolith characterization

In this section, methods adopted to characterize the monoliths were described. In particular, morphological analysis, infrared characterization, Brunauer–Emmett–Teller analysis, elemental analysis and compressive tests were performed.

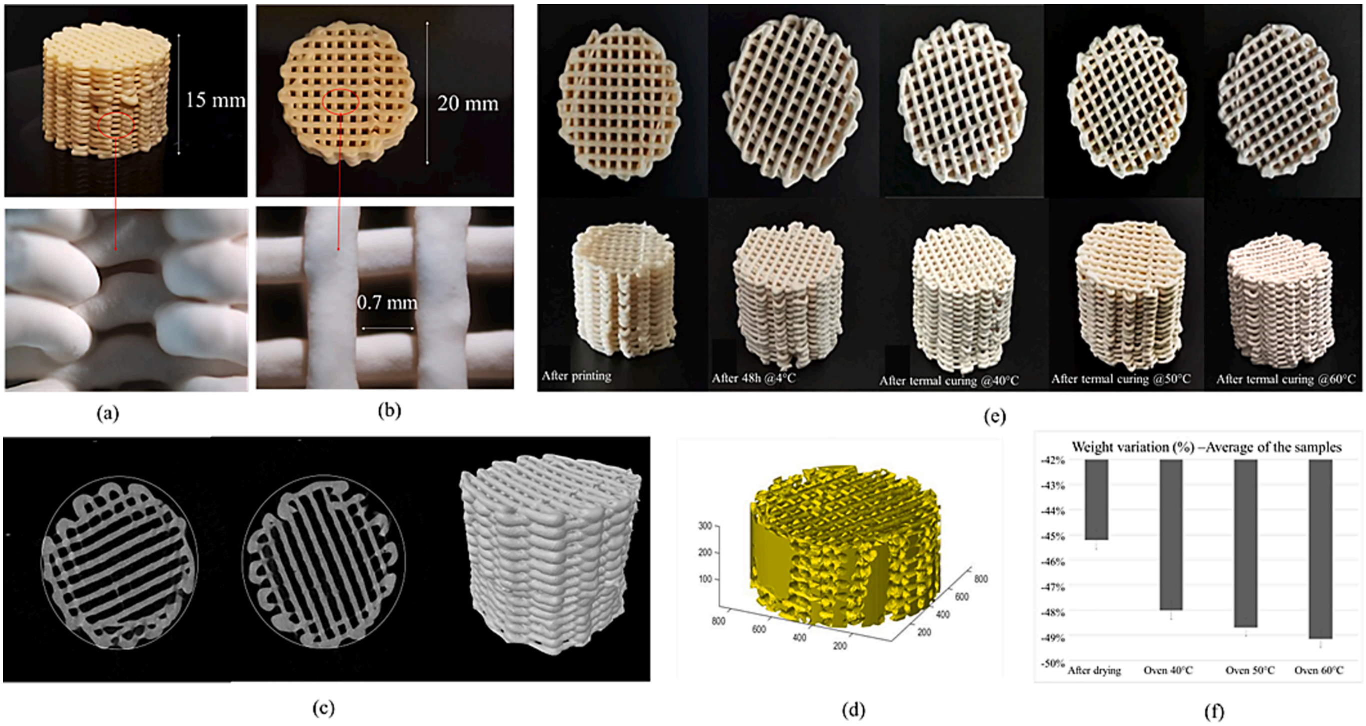

Fig. 3. (a) Self-standing 3D printed monolith Z80BLA, side view; (b) Self-standing 3D printed monolith Z80BLA, top view; (c) Morphological analysis of the Z80BLA monoliths: MicroCT section scans at different heights (the monolith perimeter is highlighted) and 3D reconstruction; (d) 3D reconstruction of the interconnected pore network; (e) Post-processing of the monoliths. For the purpose of illustration, the Z80BLA composition is selected. Pictures were taken (from left to right): just after the printing,48 h after storage at 4 °C, after thermal curing in the oven at 40 °C, 50 °C and 60 °C. The colour change is a consequence of the water content reduction; (f) Weight variation due to water loss.

3.3.1. Morphological analysis

The 3D printed monoliths were photographed using an optical microscope (Olympus A70, Japan). The macropore size and the line width were measured with ImageJ. Cross-sectional images of the monoliths were obtained by microCT (Skyscan11®, Bruker, USA) using a 0.25 mm aluminium filter, 50 kV source voltage, 800 μA source current, and a camera pixel size of 22.68 μm. During the acquisition, the monolith was rotated 360° with projection image acquisition every 1°. Projection images were reconstructed into cross-sectional images by Bruker's Nrecon® software and a 3D reconstruction of the monolith was then obtained with ®CT-analyser. Porosity, pore interconnectivity, monolith fiber width, and size of lateral and axial pores were evaluated using a script based on the Image Processing toolbox of Matlab® (The Mathworks Inc., USA) and compared with the CAD model to evaluate the shape fidelity of the 3D printed parts (Chiesa et al., 2020).

3.3.2. Infrared characterization

Fourier Transform–Infrared (FTIR) characterization of the samples was performed with a Perkin-Elmer Spectrum-Two spectrophotometer (Perkin-Elmer, Waltham, MA, USA), equipped with an Attenuated Total Reflectance (ATR) apparatus. Each spectrum consisted in 12 scans, with a resolution of 8 cm^{-1} and wavenumber range between 4000 and 450 cm^{-1}.

3.3.3. Brunauer–Emmett–Teller analysis

The specific surface area (SSA) of zeolite 13X and of the monolith samples were calculated with the Brunauer–Emmett–Teller (BET) single point method using a Gemini V Series Surface Area Analyzer (Micromeritics, Canada) through N_2 adsorption tests conducted at 77 K. Before the measurement of the specific surface area, all samples were first degassed at 423 K, to remove gases and vapours that may have become physically adsorbed onto the surface after the manufacturing process.

3.3.4. Elemental analysis

Elemental analyses were performed by the automatic analyser Elementar Vario MICRO Cube (Elementar, Italy), to quantify the amount of zeolite in monoliths, and also evaluate the reduction of carbon content after calcination. The content of organic carbon, hydrogen and nitrogen were quantified by a thermal conductivity detector (TCD).

3.3.5. Compressive test

After thermal curing, compressive tests of monolith Z80BLA (the composition selected due to its performance, see the results section) were performed in triplicate, using a universal testing machine (Zwick/Roell, Germany) equipped with a 100 N load cell. The monoliths were first polished with sandpaper (3 M, superfine grit) to smooth and flatten the surface for ensuring proper contact with the tester platen. They were then compressed at 25 %/min strain rate until break. A stress–strain curve was derived from these data and the Feret dimensions of the monolith, allowing estimation of the elastic modulus [Pa], failure stress [Pa] and strain (%), and toughness [J/m^3].

3.4. Testing of the monoliths using a commercial oxygen concentrator

The performance of monoliths was tested using an OSD® 525KS oxygen concentrator from DeVilbiss Healthcare, which nominally provides a maximum of 5 L of oxygen per minute. The oxygen concentrator has two cylinders to contain the sieve beds. One of them was left with 500 g of zeolite pellets from the original configuration. The second cylinder was filled with 140 g of 3D printed Z80BLA monoliths. Tests were conducted in triplicate, investigating the oxygen concentration output once a day for 3 days. For comparison, the same measurements were performed with one cylinder empty and the second one with the original 500 g zeolite pellets (the "without monoliths" condition). The oxygen concentration was measured using an oxygen sensor KE-25 (Figaro, USA). The sensor has a measurement range of 0–100 % and

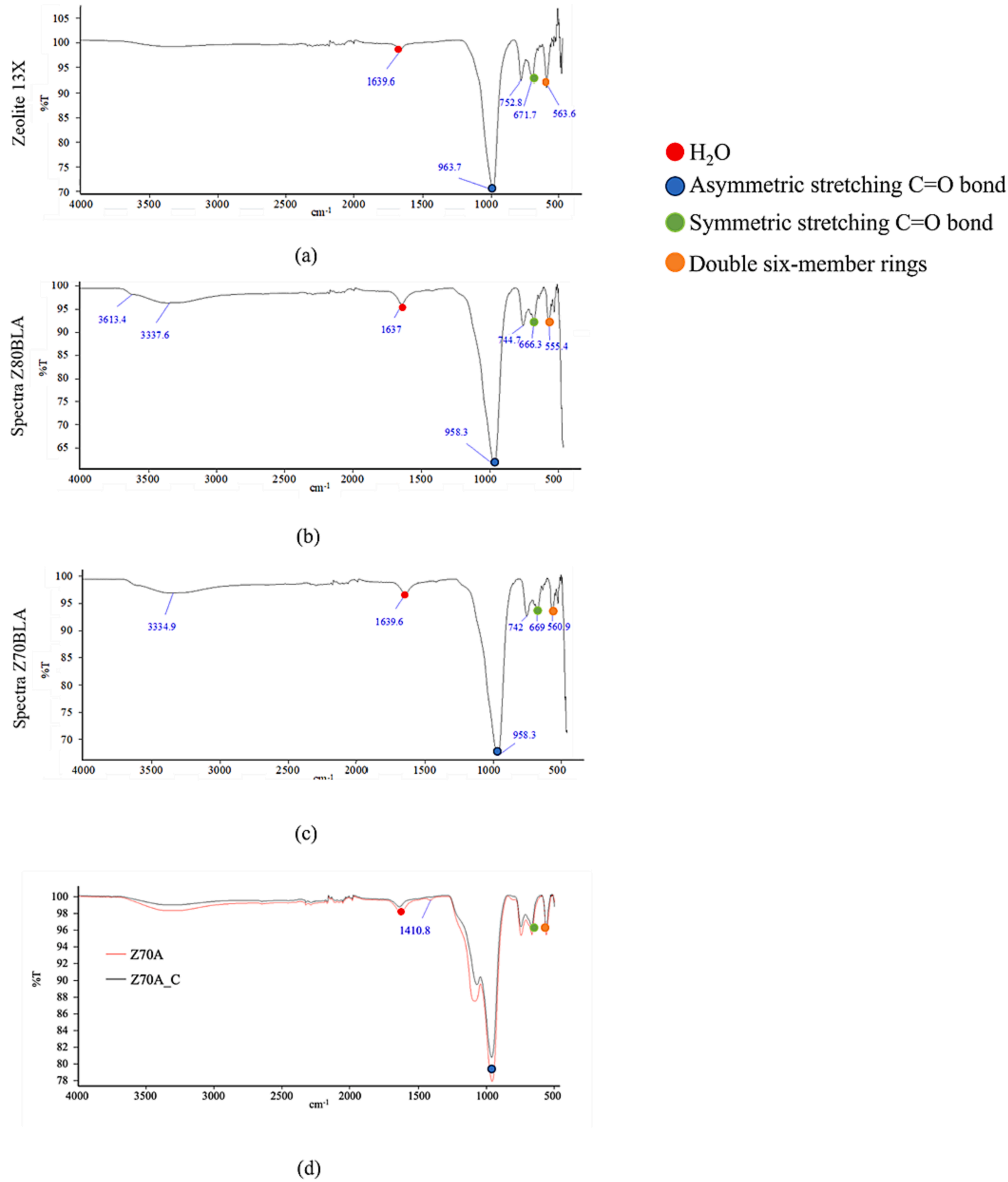

Fig. 4. (a) FT-IR spectra of zeolite 13X; (b) FT-IR spectra of Z70BLA; (c) FT-IR spectra of Z80BLA; FT-IR spectra of the two samples Z70A(red) and Z70A_C(black). Red, blue, green and orange dots highlight the contribute of H_2O, asymmetric stretching of C = O bond, symmetric stretching of C = O bond and double six member rings.

Table 2
BET single point area for selected samples ([a]: determined based on elemental analysis).

	Zeolite pellet	Z70A	Z70A_C	Z70BLA	Z80BLA
Zeolite in the monolith (wt%)[a]	100	95.9	99.1	85.3	90.9
BET surface area (m^2/g)	498.1	380.0	378.8	305.8	399.2
Normalized BET surface area (m^2/g of zeolite)	–	396.2	382.2	358.5	439.1

an accuracy of ± 1 % (full scale). It was connected to one of the cylinders of the oxygen concentrator via a 3D printed pipe (Fig. S2 in Supplementary Material).

4. Results and discussion

4.1. 3D printing process

The initial screening for selecting the zeolite/binder composition with the best performance was carried out by evaluating the printability of the slurry, that is its ability to form a structure with a free-standing well-defined architecture (Bonatti et al., 2021; Chiesa et al., 2020; Lapomarda et al., 2021). In fact, the binder system should provide the desired mechanical strength to prevent the collapse of pores in the external perimeter of the structure. Fig. 3 shows the self-standing monolith Z80BLA, with uniform square channels and layer thickness. The structure presented also pores in the XZ and YZ planes (cf. Fig. 1) allowing enhanced air transport respect to structures fabricated by the conventional extrusion process. The material combinations not presenting the ability to self-retain their shape once extruded were not further characterized. In particular, the compositions containing alginate without binders were not able to maintain lateral pores in the XZ and. YZ planes as the vertical columns collapsed under the weight of the slurry. On average, bentonite-based monoliths presented a pore size of 0.7 mm, which is the same diameter as the nozzle and, therefore coherent with the printing parameters and the fabrication setup.

4.2. Morphological analysis

MicroCT scan image analysis revealed that the monoliths' pore network is generally interconnected, with a porosity of approximately 50 %. No collapse between layers with different printing orientations was visible in bentonite-based monoliths (Fig. 3(c)). A 3D reconstruction of the structure obtained by packing MicroCT images is shown in Fig. 3 (d).

4.3. Thermal curing

Fig. 3(e) illustrates the influence of the thermal curing on the weight of the monoliths, which reached a plateau between 50 and 60 °C. No visible changes in morphology were noted. This process allows slowing down the condensation and prevents defects and cracks induced by shrinkage and strain due to rapid or irregular loss of water from the structure.

4.4. Infrared characterization and elemental analysis

FT-IR spectra analysis in all the synthesized monolith samples highlighted that the characteristic bands due to zeolite 13X are prevalent. They are particularly remarkable for the most performant monoliths with higher zeolite concentration, such as Z70BLA and Z80BLA. In Fig. 4(a), 4(b) and 4(c) the FT-IR spectra of zeolite 13X and of monolith Z70BLA and Z80BLA samples are compared. In these spectra, the main bands are due to asymmetric stretching (958–963 cm^{-1}), symmetric stretching (671–666 cm^{-1}), double six-member rings (D6R) (555–563 cm^{-1}) of 13X zeolite, while the bands at 1639–1637 cm^{-1} are ascribed to H_2O deformation modes due to incomplete dehydration of the samples (Chen et al., 2012).

Elemental analysis highlighted the significant reduction of carbon content after the calcination. In fact, the carbon content of Z70A_C (C: 0.29 %) is almost a fifth of that in the Z70A sample (C: 1.37) due to the thermal treating at high temperature which led to the burning of the organic binder sodium alginate (Dos Santos Araújo et al., 2019). It must be remarked that a modest amount of organic carbonaceous material is still present in the calcined sample. The disappearance of alginate is also confirmed by the comparison of the FT-IR spectra of the two samples (Fig. 4). In fact the bands between 1640 and 1650 cm^{-1} were assigned to the asymmetric stretching of the C = O bond of the carboxyl group of the alginate while the band at 1420–1410 cm^{-1} to the symmetric stretching of same C = O bond (Xiao et al., 2001). This last diagnostic band of sodium alginate at 1410.8 cm^{-1} is present in the spectrum of Z70A

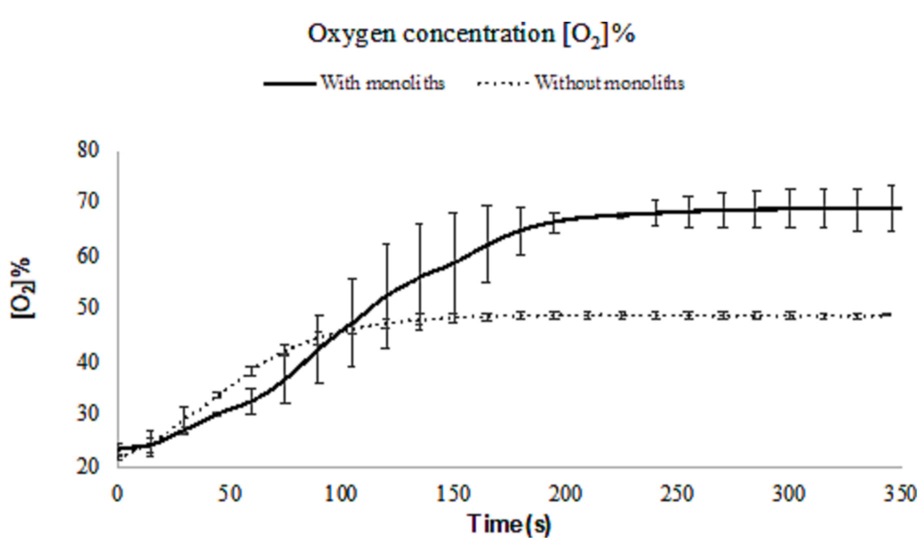

Fig. 5. Oxygen concentration during tests with (solid line) and without monoliths (dashed line) in one of the two cylinders of the oxygen concentrator OSD® 525KS. Data are reported as the average with standard deviation of three tests. For clarity, standard deviations are reported every 15 s.

(alginate content 4.1 wt%), but is not detectable in that of the calcined Z70A_C.

4.5. Brunauer-Emmett-Teller analysis

Table 2 summarizes the BET surface area of representative monolithic samples described in Table 1, characterized by different contents of the microporous zeolite 13X which has a measured surface area of 498.1 m^2/g. Owing to their lower zeolite content, the addition of the binder/plasticizer in the printed samples determines a decrease in surface area compared to the pure zeolite13X.

Remarkably, the normalization of the BET surface area to gram of zeolite present in the sample reveals that the monolith fabrication process does not significantly reduce the accessibility of the zeolite component (Table 2). Furthermore, the calcination process does not improve the BET surface area as indicated, for example, by the comparison between Z70A and Z70A_C. Among the monoliths, Z80BLA had the highest normalized BET surface area (439.1 m^2/g of zeolite).

Calcination at 600 °C does not completely remove the binders and, moreover, it has been shown by various studies that such temperatures may sometimes impact negatively to both the specific surface area and the adsorbtion properties of zeolites. For what concerns the possible role of binder, TGA analyses available in the literature for sodium alginate, as in (Flores-Hernández et al., 2021), show that some residual presence of Na_2CO_3 must be expected to occur in our monoliths even after thermal treatments at 600 °C. It is thus reasonable to speculate that some zeolite pores might have been partially blocked by small size particles of sodium carbonate. On the other end, there are also studies which show how calcinating zeolites at some hundreds of Celsius degrees may cause changes in the material and its properties. For example, Chen et al (Chen et al., 2022) reported that, up to 750 °C, the higher the calcination temperature the smaller the specific surface area of the treated zeolite sample, while Guo et al (Guo et al., 2022) observed in NaY zeolite that even the surface crystallinity, in addition to surface area, can be reduced with increasing the calcination temperature up to 700 °C, due to a partial collapse of its framework. The work of Zhang et al. underlines that the calcination process does not exert an obvious influence on the zeolite textural characteristics, a decrease of the surface area being addressed to presence of residual carbon formed during the calcination (Zhang, 2023).

4.6. Compressive test

Given its good printability and high normalized BET surface area, the 3D printed monolith Z80BLA was selected for further evaluation. Its mechanical characteristics were determined by compression tests. The monoliths have an elastic modulus of 20 ± 6 MPa and a maximum compressive stress of 450 ± 10 kPa before failure, which is higher than the maximum pressure achievable in the operating conditions of the oxygen concentrator OSD® 525KS (approx. 240 kPa). This result confirms again that the calcination process is not needed to fabricate a functional monolith, as the required mechanical strength is achieved without removing the binders through high temperature thermal treatment.

4.7. Testing of the monoliths using a commercial oxygen concentrator

The performance of the 3D printed Z80BLA monoliths was tested in the oxygen concentrator by packing them in one of two cylinders while leaving the second cylinder with the original zeolite pellets. As a control, measurements with one empty cylinder and the second one with zeolite pellets were performed in order to highlight the contribution of 3D printed monoliths.

Fig. 5 shows the oxygen concentration trends measured during tests conducted over three days (one per day) respectively with and without monoliths in one of the cylinders. Without monoliths (i.e., with an empty cylinder), the device reached an oxygen concentration of 50 ± 0.8 %. With the second cylinder filled with monoliths, the device reached an oxygen concentration value of 70 ± 4 %. Although this test must be considered more as a proof of concept than an actual validation in a real setting scenario, the results are encouraging considering that the amount of zeolite in the monoliths is about the 20 % of that contained in the pellets.

5. Conclusion

Through to a development pipeline, 3D printed monoliths were successfully fabricated, by mixing up to 80 % zeolite with a combination of binders, guaranteeing high surface area and mechanical strength. The results indicate that the calcination process does not improve the BET surface area, and the mechanical properties of the monoliths are sufficient to withstand loading during the Skarstrom cycle. Compared to the pellet raw material, the 3D printed zeolite monoliths can be easily handled and regenerated. As highlighted by the FEM models, the dynamics of airflow inside the purpose-designed channels enhanced the adsorption properties, rendering them a suitable solution for the N_2 adsorption process in oxygen concentrators. The printed structures were physically and structurally characterized and then evaluated for equilibrium and dynamic N_2 capture from air. Validation of the monoliths was performed using a commercial oxygen concentrator. The device was able to reach a maximum oxygen concentration of 70 ± 4 % due to the presence of zeolite monoliths.

The needs analysis at the basis of this research underlined that the poor availability of spare parts limits the usefulness and accessibility of oxygen concentrators in LRS. Our results show that 3D printed monoliths are good candidates for use in oxygen concentrators. The identified open-source protocol for their fabrication, supported and documented on the UBORA platform, relying on 3D printing, allows local production, even in LRS as a it requires relatively simple setup. Although further analyses are needed, such as the assessment of the durability of the monoliths under operating conditions, in a global perspective, this type of study can spur a process of reverse innovation (Malodia et al., 2020). Indeed, monoliths are more efficient in terms of specific adsorption and are less demanding in terms of power supply. These aspects can lead to lighter and thus more portable devices, which are also useful in domestic settings, whatever the context.

CRediT authorship contribution statement

Florinda Coro: Writing – review & editing, Data curation, Visualization, Investigation. **Licia Di Pietro:** Writing – original draft, Data curation, Investigation. **Simone Micalizzi:** Writing – review & editing, Data curation, Investigation. **Antonio Bertei:** Formal analysis, Validation, Writing – review & editing. **Giuseppe Gallone:** Validation, Supervision, Writing – review & editing. **Anna Maria Raspolli Galletti:** Validation, Supervision, Writing – review & editing. **Arti Ahluwalia:** Writing – review & editing, Supervision. **Carmelo De Maria:** Writing – review & editing, Conceptualization, Methodology, Validation, Supervision, Funding acquisition, Resources.

Declaration of competing interest

The authors declare that they have no known competing financial interests or personal relationships that could have appeared to influence the work reported in this paper.

Data availability

No data was used for the research described in the article.

Appendix A. Supplementary data

Supplementary data to this article can be found online at https://doi.org/10.1016/j.ces.2023.119590.

References

UBORA: Euro-Africa Open Biomedical Engineering Innovation e-platform for Innovation through Education. [Online]. Available: https://platform.ubora-biomedical.org/ [last access: April 2023].

Spare parts for oxygen concentrators - sieve beds. [Online]. Available: https://platform.ubora-biomedical.org/projects/eb64ae84-3221-4e7e-a04a-880bfe72dc82 [last access: April 2023].

Ackley, M.W., 2019. Medical oxygen concentrators: a review of progress in air separation technology. Adsorption 25 (8), 1437–1474.

Ahluwalia, A., De Maria, C., Díaz Lantada, A., 2018. The Kahawa Declaration: a manifesto for the democratization of medical technology. Global Health Innov. 1 (1), 1–4.

Ahluwalia, A., De María, C., DíazLantada, A., Di Pietro, L., Ravizza, A., Mridha, M., ... &Leivobits, A. (2018). Towards Open Source Medical Devices. Current Situation, Inspiring Advances and Challenges.

Ali, G., Fall, M., Alainachi, I., 2021. Time-and temperature-dependence of rheological properties of cemented tailings backfill with sodium silicate. J. Mater. Civ. Eng. 33 (3), 04020498.

Banks, J., 2013. Adding value in additive manufacturing: researchers in the United Kingdom and Europe look to 3D printing for customization. IEEE Pulse 4 (6), 22–26.

Bon, S.B., Chiesa, I., Morselli, D., Degli Esposti, M., Fabbri, P., De Maria, C., Valentini, L., 2021. Printable smart 3D architectures of regenerated silk on poly (3-hydroxybutyrate-co-3-hydroxyvalerate). Mater. Des. 201, 109492.

Bonatti, A.F., Chiesa, I., Vozzi, G., De Maria, C., 2021. Open-source CAD-CAM simulator of the extrusion-based bioprinting process. Bioprinting 24, e00172.

Bradley, B.D., Chow, S., Nyassi, E., Cheng, Y.L., Peel, D., Howie, S.R., 2015. A retrospective analysis of oxygen concentrator maintenance needs and costs in a low-resource setting: experience from The Gambia. Heal. Technol. 4, 319–328.

Chen, D., Hu, X., Shi, L., Cui, Q., Wang, H., Yao, H., 2012. Synthesis and characterization of zeolite X from lithium slag. Appl. Clay Sci. 59, 148–151.

Chen, X., Tao, J., Sun, P., Yu, F., Li, B., Dun, L., 2022. Effect of calcination on the adsorption of Chifeng zeolite on Pb^{2+} and Cu^{2+}. Int. J. Low-Carbon Technol. 17. https://doi.org/10.1093/ijlct/ctac006.

Chiesa, I., De Maria, C., Lapomarda, A., Fortunato, G.M., Montemurro, F., Di Gesù, R., Gottardi, R., 2020. Endothelial cells support osteogenesis in an in vitro vascularized bone model developed by 3D bioprinting. Biofabrication 12 (2), 025013.

Chueh, C.C., Bertei, A., Pharoah, J.G., Nicolella, C., 2014. Effective conductivity in random porous media with convex and non-convex porosity. Int. J. Heat Mass Transf. 71, 183–188.

Di Pietro, L., De Maria, C., Ravizza, A., Ahluwalia, A., 2019. Co-design open-source medical devices: how to minimize the human error using UBORA e-infrastructure. In: In 2019 41st Annual International Conference of the IEEE Engineering in Medicine and Biology Society (EMBC). IEEE, pp. 3730–3733.

Di Pietro, L., Piaggio, D., Oronti, I., Maccaro, A., Houessouvo, R.C., Medenou, D., Ahluwalia, A., 2020. A framework for assessing healthcare facilities in low-resource settings: field studies in Benin and Uganda. J. Med. Biol. Eng. 40 (4), 526–534.

Dos Santos Araújo, P., Belini, G.B., Mambrini, G.P., Yamaji, F.M., Waldman, W.R., 2019. Thermal degradation of calcium and sodium alginate: a greener synthesis towards calcium oxide micro/nanoparticles. Int. J. Biol. Macromol. 140, 749–760.

Enarson, P., La Vincente, S., Gie, R., Maganga, E., Chokani, C., 2008. Implementation of an oxygen concentrator system in district hospital paediatric wards throughout Malawi. Bull. World Health Organ. 86, 344–348.

Flores-Hernández, C.G., Cornejo-Villegas, M.L.A., Moreno-Martell, A., Del Real, A., 2021. Synthesis of a Biodegradable Polymer of Poly (Sodium Alginate/Ethyl Acrylate). Polymers (basel) 7;13(4):504. https://doi.org/10.3390/polym13040504.

Frame, M., & Huntley, J. S. (2012). Rapid prototyping in orthopaedic surgery: a user's guide. The Scientific World Journal, 2012.

Guo, X., Qiao, L., Zong, S., Ye, R., He, Y., Cheng, J., Cao, X., Zhou, Z., Yao, Y., 2022. ChemistrySelect 7, e202201574.

Hill, S.E., Njie, O., Sanneh, M., Jallow, M., Peel, D., Njie, M., Howie, S.R.C., 2009. Oxygen for treatment of severe pneumonia in The Gambia, West Africa: a situational analysis. Int. J. Tuberc. Lung Dis. 13 (5), 587–593.

Comsol Inc., Comsol Multiphysics user's guide, version 6.1, Burlington, MA, 2019.

Lapomarda, A., Pulidori, E., Cerqueni, G., Chiesa, I., De Blasi, M., Geven, M.A., De Maria, C., 2021. Pectin as rheology modifier of a gelatin-based biomaterial ink. Materials 14 (11), 3109.

Li, Y.Y., Perera, S.P., Crittenden, B.D., 1998. Zeolite monoliths for air separation: part 1: manufacture and characterization. Chem. Eng. Res. Des. 76 (8), 921–930.

Li, Y.Y., Perera, S.P., Crittenden, B.D., 1998. Zeolite monoliths for air separation: Part 2: Oxygen enrichment, pressure drop and pressurization. Chem. Eng. Res. Des. 76 (8), 931–941.

Liu, J., Shang, H., Yang, J., Wang, J., Li, J., Deng, S., 2021. Novel zeolite/carbon monolith adsorbents for efficient CH4/N2 separation. Chem. Eng. J. 426, 130163.

Mahaisavariya, B., Sitthiseripratip, K., Oris, P., Tongdee, T., 2006. Rapid prototyping model for surgical planning of corrective osteotomy for cubitus varus: report of two cases. Injury Extra 37 (5), 176–180.

Malkin, R.A., 2007. Design of health care technologies for the developing world. Annu. Rev. Biomed. Eng. 9, 567–587.

Malkin, R.A., 2007. Barriers for medical devices for the developing world. Expert Rev. Med. Devices 4 (6), 759–763.

Malodia, S., Gupta, S., Jaiswal, A.K., 2020. Reverse innovation: a conceptual framework. J. Acad. Mark. Sci. 48, 1009–1029.

Mosca, A., Hedlund, J., Webley, P.A., Grahn, M., Rezaei, F., 2010. Structured zeolite NaX coatings on ceramic cordierite monolith supports for PSA applications. Microporous Mesoporous Mater. 130 (1–3), 38–48.

Piaggio, D., Medenou, D., Houessouvo, R.C., Pecchia, L., 2019. Donation of Medical Devices in Low-Income Countries: Preliminary Results from Field Studies. IFMBE Proc.

Rengier, F., Mehndiratta, A., Von Tengg-Kobligk, H., Zechmann, C.M., Unterhinninghofen, R., Kauczor, H.U., Giesel, F.L., 2010. 3D printing based on imaging data: review of medical applications. Int. J. Comput. Assist. Radiol. Surg. 5 (4), 335–341.

Rezaei, F., Webley, P., 2010. Structured adsorbents in gas separation processes. Sep. Purif. Technol. 70 (3), 243–256.

Rezaei, F., Mosca, A., Webley, P., Hedlund, J., Xiao, P., 2010. Comparison of traditional and structured adsorbents for CO2 separation by vacuum-swing adsorption. Ind. Eng. Chem. Res. 49 (10), 4832–4841.

Richards-Kortum, R., Oden, M., 2013. Devices for low-resource health care. Science 342 (6162), 1055–1057.

Occupational Safety and Health Administration. (2010). Occupational exposure to respirable crystalline silica—review of health effects literature and preliminary quantitative risk assessment. OSHA: Washington, DC, USA.

Sami, A., Irfan, M., Uddin, R., Ali, A.H., Khan, H., Khan, E., Sameer, M., 2022. Oxygen concentrator design: zeolite based pressure swing adsorption. Eng. Proc. 20 (1), 26.

Schubert, C., Van Langeveld, M.C., Donoso, L.A., 2014. Innovations in 3D printing: a 3D overview from optics to organs. Br. J. Ophthalmol. 98 (2), 159–161.

Sheth, U., Theodoropoulos, J., Abouali, J., 2015. Use of 3-dimensional printing for preoperative planning in the treatment of recurrent anterior shoulder instability. Arthrosc. Tech. 4 (4), e311–e316.

Sircar, S., 2002. Pressure swing adsorption. Ind. Eng. Chem. Res. 41 (6), 1389–1392.

Thakkar, H., Eastman, S., Hajari, A., Rownaghi, A.A., Knox, J.C., Rezaei, F., 2016. 3D-printed zeolite monoliths for CO2 removal from enclosed environments. ACS Appl. Mater. Interfaces 8 (41), 27753–27761.

Thakkar, H., Lawson, S., Rownaghi, A.A., Rezaei, F., 2018. Development of 3D-printed polymer-zeolite composite monoliths for gas separation. Chem. Eng. J. 348, 109–116.

Von Seckendorff, J., Hinrichsen, O., 2021. Review on the structure of random packed-beds. Can. J. Chem. Eng. 99, S703–S733.

Wandi, F., Peel, D., Duke, T., 2006. Hypoxaemia among children in rural hospitals in Papua New Guinea: epidemiology and resource availability—a study to support a national oxygen programme. Ann. Tropicalpaediatr. 26 (4), 277–284.

Wang, H., Yang, X., Li, Z., Liu, Y., Zhang, C., Ma, X., Li, C., 2020. 3-D Modeling of Gas-Solid Two-Phase Flow in a π-Shaped Centripetal Radial Flow Adsorber. Appl. Sci. 10 (2), 614.

World Health Organization. (2016). Technical Specifications for Oxygen Concentrators: WHO Medical Device Technical Series.

World Health Organization. (2020). Priority medical devices list for the COVID-19 response and associated technical specifications.

Xiao, C., Liu, H., Lu, Y., Zhang, L., 2001. Blend films from sodium alginate and gelatin solutions. J. Macromol. Sci. Pure Appl. Chem. 38, 317.

Zaman, E., Jalali, P., 2010. On hydraulic permeability of random packs of monodisperse spheres: Direct flow simulations versus correlations. Phys. A 389 (2), 205–214.

Zapata Ballesteros, A., De Witte, N., Denayer, J.F., Van Assche, T.R., 2022. Effect of pellet size on PSA performance: monolayer and multilayer bed case study for biogas upgrading. Adsorption 28 (5–6), 197–208.

Zhang, Y., et al., 2023. Adv. Mater. Technol. 8, 2300699. https://doi.org/10.1002/admt.202300699.

Zhou, H., Bhaduri, S.B., 2019. 3D printing in the research and development of medical devices. In: Biomaterials in Translational Medicine. Academic Press, pp. 269–289.